Microsc. Microanal. 8 (Suppl. 2), 2002
DOI 10.1017.S1431927602106325

Crystallographic Analysis of Orientational Variants in $PbZr_{0.52}Ti_{0.48}O_3$ Ferroelectric Perovskite

Lijun Wu*, Yimei Zhu*, Jianqi Li* and B. Noheda**

* Department of Materials Science, Brookhaven National Laboratory, Upton, NY 11973
** Department of Physics, Brookhaven National Laboratory, Upton, NY 11973

The ferroelectric perovskite $PbZr_{1-x}Ti_xO_3$ has been extensively studied due to its unique physical properties. It exhibits an unusual morphotropic phase boundary (MPB) which divides the regions with rhombohedral and tetragonal symmetry in its phase diagram. Upon cooling, $PbZr_{0.52}Ti_{0.48}O_3$ (PZT) undergoes a ferroelectric transition from cubic (C) to tetragonal (T) at about 600K. Recently, a tetragonal to monoclinic (M) phase transition was discovered at about 300K, revealing new characteristics of the MPB [1]. The relationship between T and M follows: $a_m \sim a_T+b_T$, $b_m \sim -a_T+b_T$, $c_m \sim c_T$. In this short presentation, we report twin structures formed during the transition of C to T and T to M in PZT at room temperature using transmission electron microscopy (TEM).

The transition from C to T in PZT results in the crystal symmetric change from $Pm\bar{3}m$ to P4mm with the loss of point symmetry elements. The point group of the C phase is G= $m\bar{3}m$, while that of the T phase is H=4mm, where H of order q (q=8) is a subgroup of G, of order p (p=48). So six orientation variants are expected in the T phase. Table 1 lists all variants with their corresponding symmetry operations. The M phase has 4 orientation variants with respect to the T phase since its point group is H=Cm of order r=2. Because the M phase will inherit the variants from the T phase, it has totally 24 variants with respect to the C phase.

Fig.1(a) shows a typical morphology of the T phase. Three variants TV_1, TV_2 and TV_6 are present. Considering TV_1 as the matrix, the TV_2 is the $(\bar{1}01)$ reflection twin, while the TV_6 is the $(\bar{1}01)(101)$ secondary twin. Fig.1(b) and (c) are, respectively, the high resolution image (HREM) and its corresponding electron diffraction pattern (EDP) viewed along $[010]_{TV1}/[001]_{TV3}$ direction of the TV_1 and TV_3 variants. The boundary $(0\bar{1}1)$ plane is inclined ~46°. The displacement of Zr/Ti along c-axis can be seen in the insert I1. The simulation by multislice method in insert I1' shows that the displacement of Zr/Ti along c-axis is bigger than that measured by x-ray diffraction [1]. Furthermore, TEM experiments showed that the displacement of Zr/Ti varies from grain to grain. Thus the smaller displacement value measured by x-ray diffraction is likely due to the nature of the volume averaged x-ray probe.

The room temperature monoclinic phase is shown in fig.2. The HREM (fig.2a) is rotated 45° with respect to its EDP (fig.2b). Two variants MV_1 and MV_3 are present in fig.2 with $(\bar{1}\bar{1}1)$ reflection twin relationship. The EDP of the M phase is similar to that of the T phase but the spots of the $h\bar{h}0$ row in the former split while those of the corresponding row in the latter do not. Similar to that of the T phase, the displacement of the Zr/Ti along the a and c axes can also be observed (fig.2a). The displacement of Zr/Ti along the a and c axes were determined by comparison with the image simulation. They were found to be 0.029 and 0.037 nm, respectively, which are slightly larger than those measured by x-ray diffraction.

References:

[1] B. Noheda et al, Phys. Rev. B, 61 (2001) 8687.
[2] Work supported by US DOE under contract No. DE-AC02-98CH10886.

TABLE 1 Orientation variants and the essential operations in cosets of the T phase.

Variant	Coset	Essential operations in coset
$TV_1[001]$	H=P4mm	1, 2[001], 4^+[001], 4^-[001], m[010], m[110], m[$1\bar{1}0$], m[100]
$TV_2[100]$	m[$\bar{1}01$]	m[$\bar{1}01$], $\bar{4}^-$[010], $\bar{3}^+$[$1\bar{1}\bar{1}$], $\bar{3}^+$[$\bar{1}\bar{1}1$], 2[101], 3^+[$\bar{1}1\bar{1}$], 3^+[111], 4^+[010]
$TV_3[010]$	m[$0\bar{1}1$]	m[$0\bar{1}1$], $\bar{4}^+$[100], $\bar{3}^-$[$\bar{1}\bar{1}1$], $\bar{3}^-$[$\bar{1}1\bar{1}$] , 4^-[100], 3^-[$1\bar{1}\bar{1}$], 3^-[111], 2[011]
$TV_4[\bar{1}00]$	m[101]	m[101], $\bar{4}^+$[010], $\bar{3}^+$[$\bar{1}1\bar{1}$], $\bar{3}^+$[111], 2[$\bar{1}$01], 3^+[$1\bar{1}\bar{1}$], 3^+[$\bar{1}\bar{1}1$], 4^-[010]
$TV_5[0\bar{1}0]$	m[011]	m[011], $\bar{4}^-$[100], $\bar{3}^-$[111], $\bar{3}^-$[$1\bar{1}\bar{1}$], 4^+[100], 3^-[$\bar{1}1\bar{1}$], 3^-[$\bar{1}\bar{1}1$], 2[$0\bar{1}1$]
$TV_6[00\bar{1}]$	m[001]	m[001], $\bar{1}$, $\bar{4}^-$[001], $\bar{4}^+$[001], 2[100], 2[$\bar{1}$10], 2[110], 2[010]

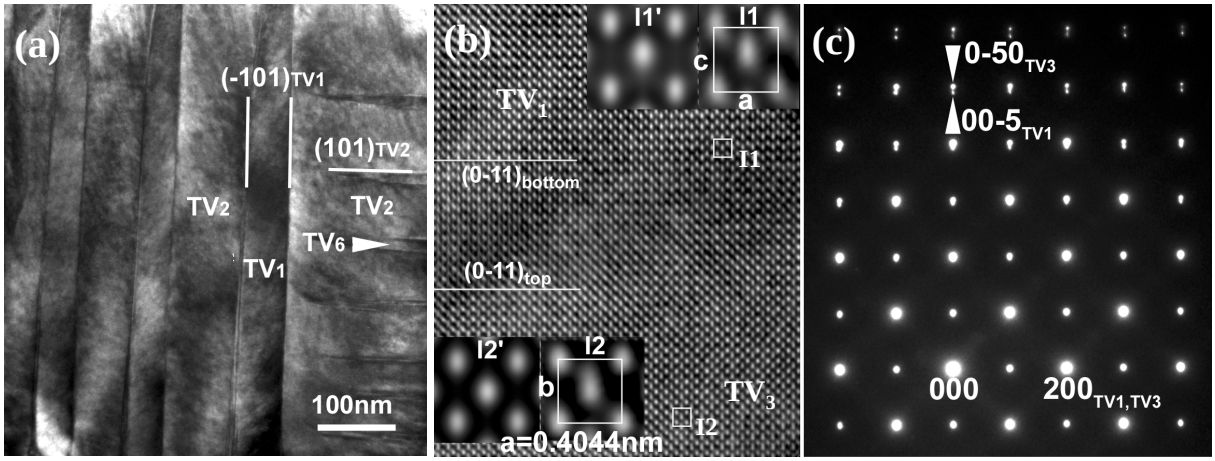

FIG.1. (a) A typical morphology of the tetragonal phase, the twins are clearly seen. The $(\bar{1}01)_{TV1}$ boundary between TV_1 and TV_2, and the $(101)_{TV2}$ boundary between TV_2 and TV_6 are both viewed edge on. (b,c) High resolution image (b) and its corresponding electron diffraction pattern (c) viewed along $[010]_{TV1}$/ $[001]_{TV3}$ direction. The twin is the $(0\bar{1}1)$ reflection twin. The twin plane $(0\bar{1}1)$ is inclined ~46°. The inserts are magnified images of the boxed areas I1 and I2, while I1' and I2' are the simulation.

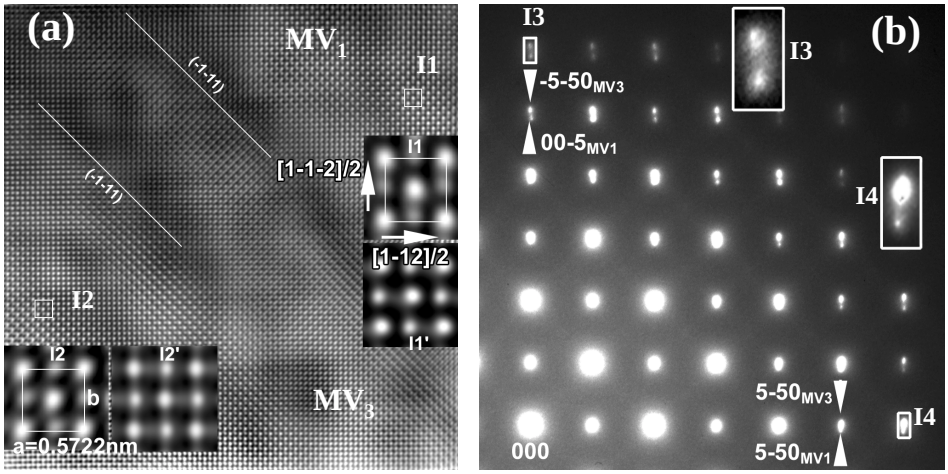

FIG.2. A high resolution image (a) and its corresponding diffraction pattern (b) of the monoclinic phase viewed along $[110]_{MV1}$/ $[001]_{MV3}$ direction. Note, the high resolution image rotates 45° with respect to the diffraction pattern. The MV_3 is the $(\bar{1}\bar{1}1)$ reflection twin. The twin plane $(\bar{1}\bar{1}1)$ is inclined ~46°. The inserts are magnified pictures from the boxed areas, while I1' and I2' are the simulation. The diffraction pattern in fig.2b is similar to that in fig.1c except splitting of the spots in $h\bar{h}0$ row.

https://doi.org/10.1017/S1431927602106325 Published online by Cambridge University Press